

Molecular Basis of the Dynamic Structure of the TIM23 Complex in the Mitochondrial Intermembrane Space

Rakhi Bajaj,¹ Łukasz Jarekko,^{1,2} Mariusz Jarekko,¹ Stefan Becker,¹ and Markus Zweckstetter^{1,2,3,*}

¹Department of NMR-based Structural Biology, Max Planck Institute for Biophysical Chemistry, 37077 Göttingen, Germany

²German Center for Neurodegenerative Diseases (DZNE), 37077 Göttingen, Germany

³Center for the Molecular Physiology of the Brain, University Medicine Göttingen, 37073 Göttingen, Germany

*Correspondence: markus.zweckstetter@dzne.de

<http://dx.doi.org/10.1016/j.str.2014.07.015>

SUMMARY

The presequence translocase TIM23 is a highly dynamic complex in which its subunits can adopt multiple conformations and undergo association-dissociation to facilitate import of proteins into mitochondria. Despite the importance of protein-protein interactions in TIM23, little is known about the molecular details of these processes. Using nuclear magnetic resonance spectroscopy, we characterized the dynamic interaction network of the intermembrane space domains of Tim23, Tim21, Tim50, and Tom22 at single-residue level. We show that Tim23^{IMS} contains multiple sites to efficiently interact with the intermembrane space domain of Tim21 and to bind to Tim21, Tim50, and Tom22. In addition, we reveal the atomic details of the dynamic Tim23^{IMS}-Tim21^{IMS} complex. The combined data support a central role of the intermembrane space domain of Tim23 in the formation and regulation of the presequence translocase.

INTRODUCTION

More than 99% of all mitochondrial proteins are synthesized in the cytosol and traverse the mitochondrial membranes to reach their final destination (Neupert and Herrmann, 2007). Preprotein import is based on the coordinated action of hetero-oligomeric translocases in the outer (TOM) and inner (TIM) mitochondrial membrane (Bauer et al., 2000; Pfanner, 1998; Ryan and Jensen, 1995; Schatz, 1996). Sorting of preproteins to the mitochondrial matrix and the inner mitochondrial membrane is achieved by the TIM23 complex in the inner mitochondrial membrane, also known as presequence translocase (Chacinska et al., 2005; Glick et al., 1992; Hutu et al., 2008; Pfanner and Geissler, 2001; van der Laan et al., 2007, 2010; Yamamoto et al., 2002).

The presequence translocase TIM23 is a highly dynamic complex in which its subunits can adopt multiple conformations and undergo association-dissociation to facilitate preprotein import (Chacinska et al., 2005; Marom et al., 2011; Popov-Celeketić et al., 2008; Tamura et al., 2009; van der Laan et al., 2010).

TIM23 contains the core proteins Tim23, Tim17, and Tim50, as well as Mgr2 and Tim21 as accessory subunits and the motor-associated proteins Pam 17, Pam 16-18, Tim44, and mtHsp (Chacinska et al., 2009; Endo et al., 2011; Gebert et al., 2012; Kutik et al., 2007; Neupert and Herrmann, 2007; Wiedemann et al., 2004). The functional form of TIM23 involves diverse interactions between the intermembrane space (IMS) domains of its subunits that are important for: (1) receiving the presequence (de la Cruz et al., 2010; Marom et al., 2011; Moczko et al., 1997; Schulz et al., 2011), (2) formation of the translocation contact (Albrecht et al., 2006; Chacinska et al., 2003; Mokranjac et al., 2005; Shiota et al., 2011; Tamura et al., 2009), and (3) regulation of the pore across the inner membrane (Martinez-Caballero et al., 2007; Meinecke et al., 2006). Indeed, in vivo and in vitro crosslinking studies have provided support for a variety of IMS interactions such as Tim23-Tim50, Tim21-Tim23, Tom22-Tim50, Tim17-Pam18, and Pam17-Tim23 (Chacinska et al., 2005; Hutu et al., 2008; Lytovchenko et al., 2013; Marom et al., 2011; Moczko et al., 1997; Shiota et al., 2011; Tamura et al., 2009; Yamamoto et al., 2002). In addition, the incoming preprotein can be crosslinked to the IMS domains of many of the aforementioned subunits (Geissler et al., 2002; Moczko et al., 1997; Schulz et al., 2011; Shiota et al., 2011; Tamura et al., 2009).

The IMS domain of Tim23 plays a key role for preprotein import (Davis et al., 2000; Donzeau et al., 2000; Gevorkyan-Airapetov et al., 2009; Popov-Celeketić et al., 2008; Tamura et al., 2009; Truscott et al., 2001). In *Saccharomyces cerevisiae*, Tim23^{IMS} consists of the N-terminal 96 residues of Tim23. Tim23^{IMS} is intrinsically disordered in vitro and contains a binding site for presequences (de la Cruz et al., 2010). In intact mitochondria, the first 20 amino acids of Tim23^{IMS} are sensitive to protease cleavage and have been proposed to traverse the outer mitochondrial membrane. In addition, residues 50–96 of Tim23 were proposed to dimerize and regulate channel activity (Bauer et al., 1996). Crosslinks and mutations in this region affect the association with various other subunits including Tim50 and Tim21 (Gevorkyan-Airapetov et al., 2009; Tamura et al., 2009).

Despite the importance of protein-protein interactions within the TIM23 complex, little is known about the molecular details of these interactions. At present, only the 3D structure of a presequence in complex with the cytosolic domain of Tom20 has been resolved (Abe et al., 2000), whereas no 3D structure of a

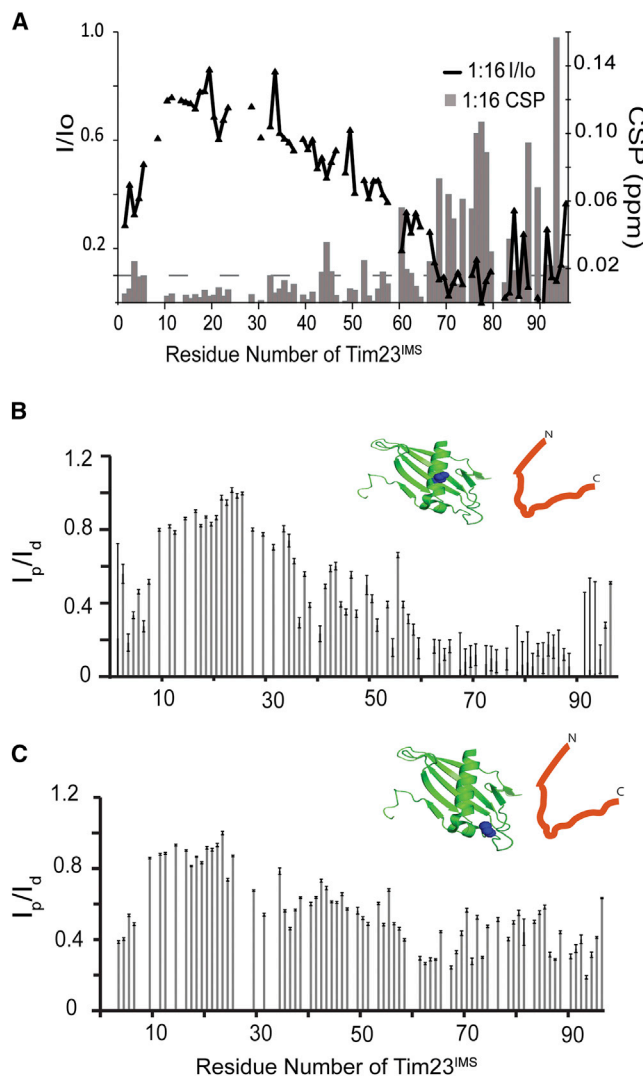


Figure 1. Single-Residue Analysis of the Binding of Tim21^{IMS} to Tim23^{IMS}

(A) Interaction sites in Tim23^{IMS} for Tim21^{IMS} as derived from 2D ¹H-¹⁵N-HSQC titration experiments of ¹⁵N-labeled Tim23^{IMS} with increasing amounts of unlabeled Tim21^{IMS}. Changes in NMR signal intensity and position at 16-fold excess of Tim21^{IMS} are shown.

(B and C) Paramagnetic relaxation enhancement induced in Tim23^{IMS} upon addition of MTSL-tagged Tim21^{IMS}. PRE profiles (ratio of signal intensities observed in 2D ¹H-¹⁵N HSQC spectra in the paramagnetic, I_p, and diamagnetic, I_d, state) as a function of Tim23 residue number upon addition of (B) Tim21^{IMS} MTSL-tagged at S114C and (C) Tim21^{IMS} MTSL-tagged at C128. Missing data points are due to the presence of prolines or signal overlap. The error in intensity ratios were based on the signal-to-noise ratio. Cartoon representations show unlabeled Tim21^{IMS} (green) and ¹⁵N-labeled Tim23^{IMS} (red) at a 1:1 molar ratio. The position of the paramagnetic tag is shown in blue.

protein-protein complex within or between the translocases is known. Here we investigated the protein interaction network of the intermembrane space domain of Tim23, the central component of the TIM23 complex, at the residue level and determined the atomic details of the Tim23^{IMS}-Tim21^{IMS} complex. The combined data support a central role of Tim23^{IMS} in the formation and dynamic regulation of the TIM23 complex.

RESULTS

Three Tim23 Sites Bind to Tim21^{IMS}

The dynamic association and dissociation of Tim21 with the core subunits of TIM23 has been proposed to regulate the sorting of the preprotein either to the inner mitochondrial membrane or to the mitochondrial matrix (Chacinska et al., 2005; van der Laan et al., 2007, 2010). In addition, Tim23^{IMS} has been crosslinked to Tim21 in vivo (Lytovchenko et al., 2013; Tamura et al., 2009). To obtain insight into the interaction of the IMS domains of Tim23 and Tim21 at single-residue resolution, we used nuclear magnetic resonance (NMR) spectroscopy. To this end, we titrated ¹⁵N-labeled Tim23^{IMS} with increasing amounts of unlabeled Tim21^{IMS}. The addition of Tim21^{IMS} caused progressive changes in NMR signal intensity and position in distinct regions of Tim23^{IMS} (Figure 1A). NMR signals of residues 67–74 and 90–96 were strongly broadened and shifted, identifying them as anchor sites for Tim21^{IMS}. In addition, residues 1–7 showed pronounced signal attenuation (Figure 1A), whereas the gradual signal decrease from residues 30 to 60 is likely due to enhanced NMR relaxation times as a consequence of binding of residues 67–74 to the globular structure of Tim21^{IMS}. To validate a direct interaction of Tim21^{IMS} with Tim23^{IMS}, we attached the paramagnetic tag MTSL to two sites in Tim21^{IMS}. The two attachment sites, 114 and 128, were in proximity to the Tim21^{IMS} residues that are involved into binding to Tim23^{IMS} (see below and Figures 1B and 1C). The MTSL-tagged Tim21^{IMS} variants were then added to Tim23^{IMS} in a 1:1 molar ratio. Pronounced PRE broadening was observed in the three regions of Tim23 (Figures 1B and 1C), which showed strong chemical shift perturbation, demonstrating a direct interaction of these regions with Tim21^{IMS}. Residues 1–7, 68–74, and 90–96 consist of the sequences MSWLF₆GD, VEYLDLE, and SRGW₇TDD, respectively. All three residue stretches contain an aromatic residue at position *i* (F5, Y70, W93) and an aspartic acid at position *i*+2. In addition, the stretches ⁶⁸VEYLDLE⁷⁴ and ⁹⁰SRGW₇TDD⁹⁶ contain at least one additional negatively charged residue, whereas an additional aromatic residue is located at the N terminus. Taken together, the data demonstrate that three distinct regions in Tim23^{IMS} participate in complex formation with Tim21^{IMS}.

Rapid Exchange of Tim23 Sites with a Single Tim21 Binding Pocket

Next, we identified the binding site of Tim23^{IMS} on Tim21^{IMS}. Concentration-dependent changes in NMR chemical shifts were observed for the Tim21^{IMS} residues F109, V113, S114, V116 and E117, and 138–144 upon addition of Tim23^{IMS} (Figure 2A). Quantitative analysis of the binding curves determined the K_d value as 153 ± 67 μM. Notably, surface plasmon resonance of immobilized Tim23^{IMS} pointed to a much lower K_d of ~1 μM (Lytovchenko et al., 2013). However, because Tim23^{IMS} is known to bind to hydrophobic environments such as membranes (Donzeau et al., 2000) and the Tim23^{IMS}-Tim21^{IMS} interaction involves three Tim23 segments that are in rapid exchange (Figure 1), analysis of the interaction by surface plasmon resonance is complicated. The residues identified with NMR analysis are located in β strand 1 and on one side of the α helix 1 of

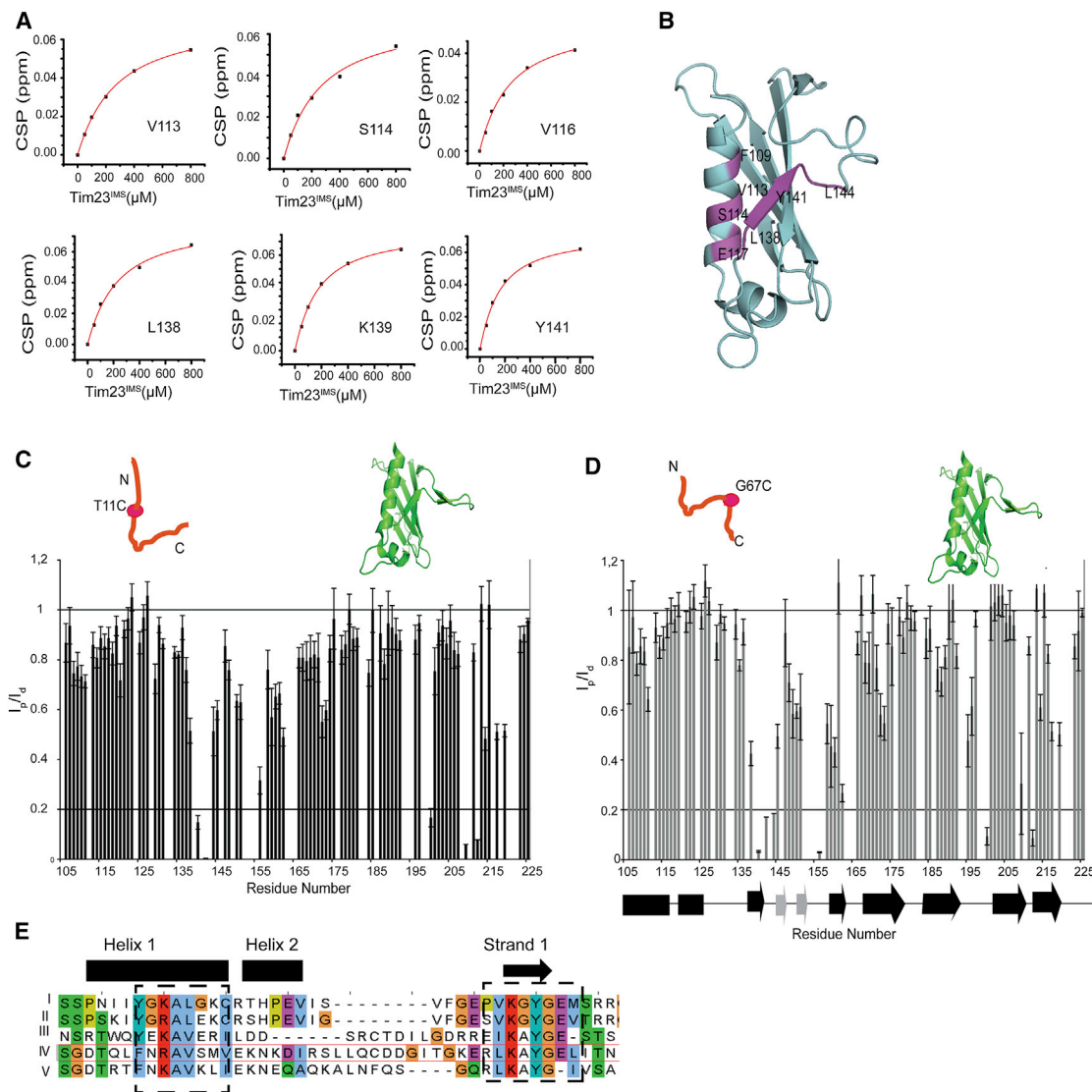


Figure 2. Tim23^{IMS} Binds to a Conserved Pocket in Tim21^{IMS}

(A) Residue specific binding curves of Tim21^{IMS} residues belonging to helix 1 and β strand 1. Chemical shift changes were fit to a single site model.

(B) Localization of the Tim23-binding site on the solution structure of Tim21^{IMS}. Residues experiencing strong NMR signal perturbation upon addition of Tim23 are shown in magenta.

(C and D) Paramagnetic relaxation enhancement induced in Tim21^{IMS} (green) upon addition of MTSL-tagged Tim23^{IMS} (red). Tim23^{IMS} was tagged with MTSL at position T11C (C) and G67C (D). I_p/I_d are the intensity ratios obtained from 2D ¹⁵H-¹⁵N HSQC spectra of Tim21^{IMS} in the presence of MTSL-tagged Tim23^{IMS} (I_p) and after addition of ascorbic acid to the same sample (I_d). Missing data points are due to the presence of prolines or signal overlap. In (D), the location of secondary structure elements in Tim21^{IMS} is indicated. The β hairpin seen in the crystal but absent in solution (see Figure 3) is shown in gray. The most strongly attenuated residues were 138–144, defining the binding pocket in Tim21^{IMS}. The errors in intensity ratios were based on signal-to-noise ratio.

(E) Sequence alignment for Tim21^{IMS} highlighting the conservation of residues in the Tim23^{IMS} binding site among different kingdoms with I-V as *Rattus norvegicus*, *Homo sapiens*, *Aspergillus flavus*, *Saccharomyces cerevisiae*, and *Candida albicans*, respectively. The sequence alignment was done using ClustalW (Larkin et al., 2007) and depicted with Jalview (Clamp et al., 2004). Hydrophobic and aromatic residues are highlighted in blue; positive and negative charged as red and magenta, respectively; neutral residues in green; glycine and proline in orange and yellow, respectively. (Top) Secondary structure elements of *S. cerevisiae* Tim21 are shown and the dashed box highlights the Tim23^{IMS} binding region in Tim21^{IMS}.

Tim21^{IMS} (Figure 2B). Further support for the rapid exchange of multiple binding motifs of Tim23^{IMS} with a common Tim21 binding site was provided by paramagnetic relaxation enhancement: attachment of a MTSL-tag to either residue 11 of Tim23, i.e., the N-terminal binding region of Tim23, or residue 67, which is in proximity to the binding region 2 in Tim23, caused highly similar

paramagnetic broadening in Tim21^{IMS} (Figures 2C and 2D). The Tim21^{IMS} residues that form the shallow binding pocket for binding to Tim23^{IMS} are conserved (Figure 2E).

The striking finding of the NMR-based interaction mapping is that three regions in Tim23^{IMS} are involved in binding, but on Tim21^{IMS} there is only a single binding site. To further support

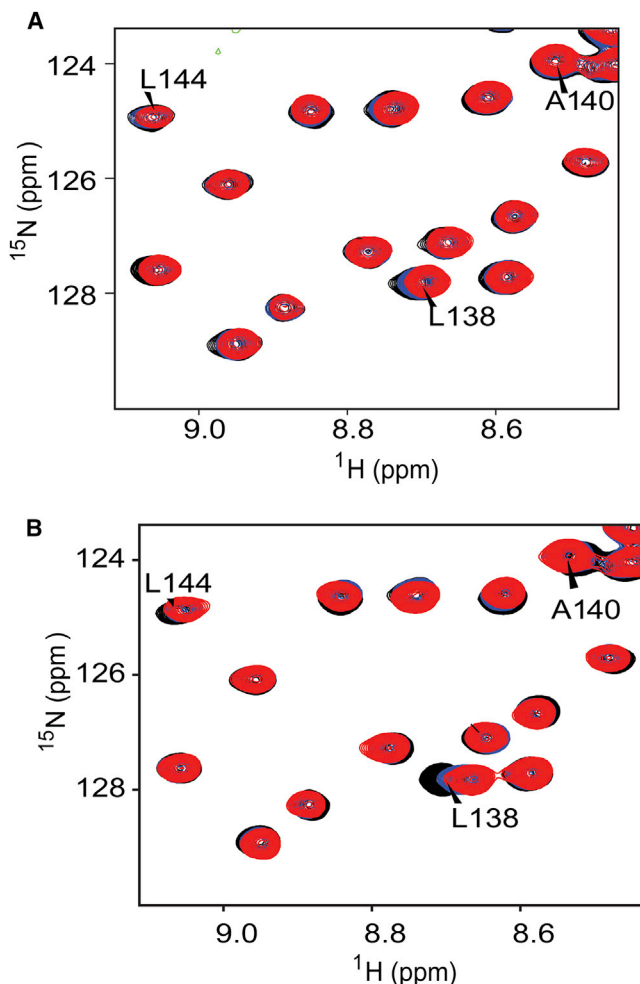


Figure 3. Interaction of Linear Motifs of Tim23^{IMS} with Tim21^{IMS}
 Superposition of selected regions of 2D ¹H-¹⁵N HSQC spectra of Tim21^{IMS} with increasing amounts of Tim23(1–13) (A) and Tim23(61–96) (B), respectively (reference, black; 8-fold excess, blue; and 32-fold excess, red).

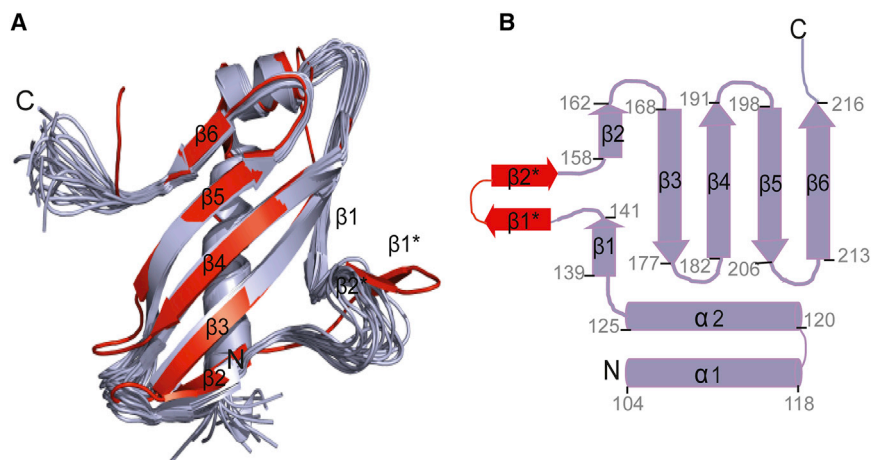
the complex nature of this interaction, we analyzed the Tim21^{IMS} interaction of a peptide comprising the N-terminal 13 residues of Tim23 (Figure 3A). In addition, in a separate experiment, the binding of a peptide comprising residues 61–96 of Tim23^{IMS} to Tim21^{IMS} was measured (Figure 3B). Tim23(1–13) contains the N-terminal Tim21-binding site, whereas Tim23(61–96) contains the other two interacting residue stretches. Stepwise addition of each of the Tim23 fragments caused the same chemical shift trajectories of Tim21^{IMS} residues as observed in the binding studies with the full Tim23^{IMS} domain (Figures 3A and 3B). However, the magnitude of chemical shift changes was significantly smaller in case of the peptides. Quantitative analysis indicated a K_d of $396 \pm 65 \mu\text{M}$ for Tim23(61–96), that is approximately 2-fold higher than that of Tim23(1–96) (Figure S1 available online). In the case of Tim23(1–13), NMR signal perturbation was even smaller, pointing to a K_d value exceeding 1 mM. The observation that the Tim23 fragments change the position of individual NMR signals of Tim21^{IMS} in the same direction as the complete IMS domain proves that the three binding motifs of Tim23^{IMS} bind

in a similar manner to the same site in Tim21^{IMS}. In addition, due to the similarity of the chemical shift changes, we further conclude that the Tim21-binding mode of Tim23(1–13) is highly similar to that of residues 69–74 and 90–96, albeit at a decreased affinity. Thus, rapid exchange of multiple Tim23 binding sites with a single Tim21 binding pocket is essential for an effective Tim23^{IMS}-Tim21^{IMS} association.

Dynamic Structure of the Tim21^{IMS}-Tim23^{IMS} Complex

To obtain an atomic resolution view of the association of Tim23^{IMS} with Tim21^{IMS}, we characterized the 3D structure of Tim21^{IMS} in complex with the three Tim23 binding motifs. This was achieved by determination of the solution structure of Tim21^{IMS}, followed by NMR-driven docking of the Tim23^{IMS} binding motifs. The 3D structure of unbound Tim21^{IMS} was determined based on nearly complete chemical shift assignment and a large number of nuclear Overhauser effect (NOE) distance restraints (Figure 4 and Table 1). Comparison of the solution structure of Tim21^{IMS} with the one observed in the crystal (Albrecht et al., 2006) showed that the core of the structures is highly similar. However, residues 144–153, which are in spatial proximity to the Tim23 binding site (Figure 2), do not form a β hairpin in solution but are dynamic (Figure 4B). Indeed, residues 144–153 are involved in crystal contacts that can stabilize the β hairpin. We then used the NMR chemical shift perturbation and paramagnetic broadening data to dock the three binding motifs of Tim23—that is, ¹MSWLFGD⁷, ⁶⁸VEYLDLE⁷⁴, and ⁹⁰SRGWTD⁹⁶—to the Tim21^{IMS} solution structure. Because of the low affinity of each individual motif, no large structural rearrangements are expected to occur in Tim21^{IMS} upon binding of Tim23^{IMS}. For docking, the Tim23 peptide was positioned in an extended conformation 10–12 Å above the binding pocket as defined by the NMR data. Peptide docking was performed, in which the structure of Tim21^{IMS} was kept fixed but the structure of the Tim23-motif was allowed to change. Figures 5A and S2 show different docked conformations of the three Tim23 motifs in complex with Tim21^{IMS}. Due to the dynamic nature of the Tim23^{IMS}-Tim21^{IMS} complex, it was not possible to obtain experimental information about the structure of the three Tim23^{IMS} binding motifs when bound to Tim21^{IMS}. Thus, we cannot exclude that the three Tim23^{IMS} motifs can also populate alternative conformations. Despite this uncertainty, however, the docking models shown in Figures 5A and S2 suggest that K139 and Y141 of Tim21 might be important for the interaction with Tim23^{IMS}.

Notably, peptide docking did not result in a single bound conformation, but a set of conformations with similar docking energies. Moreover, even for a single Tim23 binding motif, different hydrophobic residues formed contacts with Y141 of Tim21^{IMS} in the docked structures (Figures 5A and S2). Part of this structural heterogeneity might be due to limitations of the docking algorithm. On the other hand, experimental support for structural heterogeneity in the Tim23^{IMS}-Tim21^{IMS} complex comes from PRE-broadening induced in Tim21^{IMS} upon addition of Tim23^{IMS}, which was tagged with MTSL at either residue 11 or 67 (Figures 2C and 2D). The MTSL attachment site (residue 11) is in one case C terminal to the binding motif (the ¹MSWLFGD⁷ motif), whereas in the other case (residue 67), it is N terminal to the ⁶⁸VEYLDLE⁷⁴ binding motif. The PRE profiles

**Figure 4. Solution Structure of Tim21^{IMS}**

(A) Superposition of the 20 lowest energy NMR conformers (purple) of Tim21^{IMS} with the X-ray structure (red; Protein Data Bank code: 2CIU; Albrecht et al., 2006).

(B) Secondary structure of Tim21^{IMS}. Residue numbers are marked. Note that in solution, residues 145–154 are flexible and do not form a beta hairpin (beta 1* and beta 2*) as seen in the crystal. Residues 145–154 are in immediate vicinity to the Tim23^{IMS} binding site.

induced in Tim21^{IMS} were, however, similar (Figures 2C and 2D), a finding not expected when each motif would bind in a single orientation (as in this case the MTSL tag would likely be located at different sites with respect to Tim21^{IMS}). Conformational heterogeneity might be important for the ability of Tim21^{IMS} to recognize the three different Tim23 binding motifs (Figure 5B). In addition, it might allow for lower affinity and therefore efficient dissociation despite the specificity of the Tim23-Tim21 interaction.

Interaction of Tim23 with Tim50

Within the TIM23 complex, the association of the IMS domains of Tim23 and Tim50 plays an important role in receiving the presequence carrying preprotein from the outer mitochondrial translocase and directing it to the inner mitochondrial pore (Meinecke et al., 2006; Shiota et al., 2011). In vitro binding studies in combination with in vivo chemical crosslinking revealed that Y70 and L71 of Tim23^{IMS} are important for binding to Tim50^{IMS} (Gevorgyan-Airapetov et al., 2009; Mokranjac et al., 2003; Tamura et al., 2009; Yamamoto et al., 2002). Y70 and L71 belong to the Tim23 residue stretch ⁶⁸VEYLDLE⁷⁴ that binds to Tim21^{IMS} (Figure 5). To obtain insight into the Tim23-Tim50 interaction on a residue level, we used two different Tim50^{IMS} variants. Tim50(164–476) comprises most of the IMS domain of Tim50, whereas for Tim50(164–361), the 3D structure is known (Qian et al., 2011), but it lacks the presequence-binding domain. Complex formation between Tim23^{IMS} and Tim50(164–361) caused a strong decrease in NMR signal intensity of residues 1–7 and 56–78 of Tim23^{IMS} (Figure 6A). Because no accompanying chemical shift changes were observed, it suggests that the binding process is not fast on the NMR time scale. When using Tim50(164–476), more Tim23 residues participated in complex formation and the affinity was increased (Figure 6B). Quantitative analysis showed that the affinity of the Tim23^{IMS}-Tim50(164–476) complex in solution is 10–20 μM (Figure 6C). Taken together, the data demonstrate that efficient formation of the Tim23^{IMS}-Tim50^{IMS} complex requires the C-terminal, so-called presequence-binding domain of Tim50.

Identification of the Tim23-Tom22 Translocation Contact Site

A direct translocation contact between the TOM40 complex and the TIM23 complex has been established by in vivo cross-

linking of Tom22 to residue 41 of Tim23 (Tamura et al., 2009). Our NMR-based binding analysis of the isolated domains supports a translocation contact between Tim23 and Tom22. Tim23 residues V53 and L58–L61 were perturbed by addition of Tom22^{IMS} (Figure 7A). Moreover, changes in carbon resonances of the aliphatic side chains of Tom22^{IMS} were observed upon addition of Tim23^{IMS} (Figure 7B). Thus, both in vivo crosslinking—and in vitro binding map the Tim23-Tom22 translocation contact to the central part of Tim23^{IMS}. In contrast to the direct Tim23^{IMS}-Tom22^{IMS} interaction, NMR signals of Tim23^{IMS} remained unperturbed in a titration with the N-terminal tail of Tom40 (Figure 7C), which is predicted to be disordered and located in the IMS. In addition, we did not detect an interaction between Tim21^{IMS} and Tom22^{IMS} (Figure S3), in line with the finding that Tim21 appears not to play a primary role in linking the TOM40 and TIM23 complexes (Tamura et al., 2009).

DISCUSSION

To facilitate preprotein import, the subunits of the TIM23 complex adopt multiple conformations and undergo association-dissociation processes (Popov-Celeketić et al., 2008; van der Laan et al., 2007). The Tim23 protein is the main subunit of the presequence translocase. It forms the protein-conducting pore in the inner mitochondrial membrane (Truscott et al., 2001) and has been suggested to interact with more than 15 subunits across the translocases (Albrecht et al., 2006; Chacinska et al., 2003; Mokranjac et al., 2005; Shiota et al., 2011; Tamura et al., 2009). Interactions among the intermembrane space domains of TIM23 are important in receiving and directing the preprotein toward the TIM23 channel. Using purified IMS domains of Tim23 and Tim21 in combination with NMR spectroscopy, we revealed a complex mechanism of interaction between the intermembrane space domains of Tim23 and Tim21. Tim23 contains three distinct motifs that bind to a single binding pocket in Tim21 (Figures 1, 2, 3, 4, and 5). The binding pocket is formed by beta strand 1 and alpha helix 1, a region that is evolutionary conserved in Tim21 (Figures 2B and 2E). The Tim23 binding motifs bind individually very weakly to Tim21 (Figure 3). However, by being connected within one chain, the concentration of Tim21-binding motifs effectively increases, so that the rate of binding of Tim23 to Tim21 is enhanced.

Table 1. NMR Constraints and Structural Statistics for the Ensemble of 20 Lowest Energy Conformers of Tim21^{IMS} Calculated in Xplor-NIH 2.2.1

NOE Distance Constraints ^a	3,134
Intraresidual and sequential ($ i-j \geq 1$)	1,654
Medium range ($1 < i-j < 5$)	373
Long range ($ i-j \geq 5$)	1,107
Restraints per residue	24.7
Torsion angle constraints	
Backbone (ϕ/ψ)	95/95
Mean rmsd from experimental restraints (\pm SD)	
NOE (Å)	0.0054 \pm 0.0002
Dihedral angles (°)	0.2502 \pm 0.0003
Rmsd from idealized covalent geometry (region 1..127) (\pm SD)	
Bonds (Å)	0.0015 \pm 0.0002
Angles (°)	0.3859 \pm 0.0019
Impropers (°)	0.2200 \pm 0.0071
Ramachandran plot (1..127) ^b	
Residues in most favored regions (%)	74.4 \pm 1.4
Residues in additional allowed regions (%)	19.4 \pm 1.4
Residues in generously allowed regions (%)	5.1 \pm 1.1
Residues in disallowed regions	1.1 \pm 1.0
Ramachandran plot (5..46,57..120)	
Residues in most favored regions (%)	83.0 \pm 1.0
Residues in additional allowed regions (%)	15.8 \pm 1.0
Residues in generously allowed regions (%)	1.2 \pm 0.7
Residues in disallowed regions	0.0 \pm 0.7
Rmsd to the mean structure ^c	
Ordered backbone atoms (1..127) (Å)	2.10 \pm 0.47
Ordered heavy atoms (1..127) (Å)	2.38 \pm 0.41
Rmsd to the mean structure	
Ordered backbone atoms (5..46,57..120) (Å)	0.52 \pm 0.09
Ordered heavy atoms (5..46,57..120) (Å)	0.92 \pm 0.08

From Schwieters et al., 2003.

^aNone of the 20 structures had a distance violation more than 0.2 Å and dihedral angle violations more than 5°.

^bThe quality of the 20 Tim21^{IMS} conformers was evaluated using PROCHECK-NMR (v.3.4) (Laskowski et al., 1996).

^cRmsd values were calculated with MOLMOL (Koradi et al., 1996).

Binding of several short linear motifs to a single binding site was previously observed to regulate the interaction of the disordered cyclin-dependent kinase inhibitor Sic1 with its receptor Cdc4 (Mittag et al., 2008). Electrostatic interactions between multiple phosphorylated sites on Sic1 and Cdc4 resulted in a dynamic equilibrium. In case of Tim23^{IMS}-Tim21^{IMS} a similar dynamic complex is found (Figure 5). However, in contrast to the Sic1-Cdc4 system, hydrophobic interactions are more important for the dynamic recognition of Tim21^{IMS}. In addition, our structural analysis points to the existence of conformational heterogeneity of even a single Tim23^{IMS} motif when bound to Tim21^{IMS} (Figures 5 and S2). This feature is reminiscent of the dynamic binding mode of a presequence in the binding site of the cytoplasmic domain of Tom20 (Ko-

muro et al., 2013; Saitoh et al., 2011) and highlights the importance of dynamic interactions for protein import into mitochondria.

What is the role of the linear binding motifs of Tim23 for other IMS interactions? Residue-specific analysis of the Tim23^{IMS}-Tim50^{IMS} interaction showed that all three Tim21-binding motifs of Tim23 are also involved in binding to Tim50^{IMS} (Figure 6). In addition, the full IMS domain of Tim50 further recruits residues 29–46 of Tim23 into the complex (Figure 6B). The data show that Tim23's interaction motifs are involved in several IMS interactions. The motifs are highly conserved (Figure 8A) and can bind to multiple partners (Figure 8B). Multiple binding sites are used to enhance affinity for one protein such as Tim21 or Tim50. In addition, the presence of several distinct interaction motifs might enable simultaneous binding of the intermembrane space domain of Tim23 to multiple protein components of the TIM23 complex. Such an interaction with multiple protein partners might stabilize the TIM23 complex and potentially enable the formation of heterooligomeric complexes in the translocation contact site. The presequence binding site in Tim23 (de la Cruz et al., 2010) overlaps with one of the motifs that is important for binding to both Tim21 and Tim50 (Figures 1 and 6). Because the affinity of each of the three individual motifs in Tim23 for binding to Tim21 is weak, presequence can efficiently compete with the 68–74 motif of Tim23 for binding to Tim21^{IMS}/Tim50^{IMS}, whereas the other two motifs are still bound to either Tim21^{IMS} or Tim50^{IMS}. In this way, the TIM23 complex might be regulated in a signal-sensitive manner.

Tim23 is anchored with its C-terminal tail in the inner mitochondrial membrane and can contact the outer mitochondrial membrane through its IMS domain (Donzeau et al., 2000). Removal of the 50 residues at the N terminus of Tim23, however, only modulates preprotein import (Chacinska et al., 2003). Thus, alternative ways to coordinate the translocases of the outer and inner mitochondrial membrane must exist (Chacinska et al., 2003; de la Cruz et al., 2010; Popov-Celeketić et al., 2008; Tamura et al., 2009). Using NMR spectroscopy we demonstrated that residues 53–61 of Tim23 directly bind in vitro to Tom22^{IMS}, whereas no interaction with the C-terminal tail of Tom40 was detected (Figure 7). In line with a direct interaction between the central region of Tim23 and the IMS domain of Tom22, Tom22 has been crosslinked in vivo to residue 41 of Tim23 (Tamura et al., 2009). The region of Tim23^{IMS} that binds to Tom22^{IMS} is not involved in binding to presequence (de la Cruz et al., 2010) and does not participate in the complex with Tim21^{IMS} (Figure 8). Formation of the Tim23-Tom22 translocation contact is therefore possible even when Tim21 is associated with the TIM23 complex.

In summary, we provided residue-level insight into the interaction of the intermembrane space domains of Tim23, Tim21, and Tim50, key components of the TIM23 complex, and determined the dynamic structure of the Tim23^{IMS}-Tim21^{IMS} complex. In addition, we identified the translocation contact site between Tim23 and Tom22, a major component of the TOM40 translocase in the outer mitochondrial membrane. We showed that Tim23^{IMS} contains multiple sites to efficiently interact with the intermembrane space domain of Tim21 and to bind to multiple partners. Our data support a central role of the intermembrane

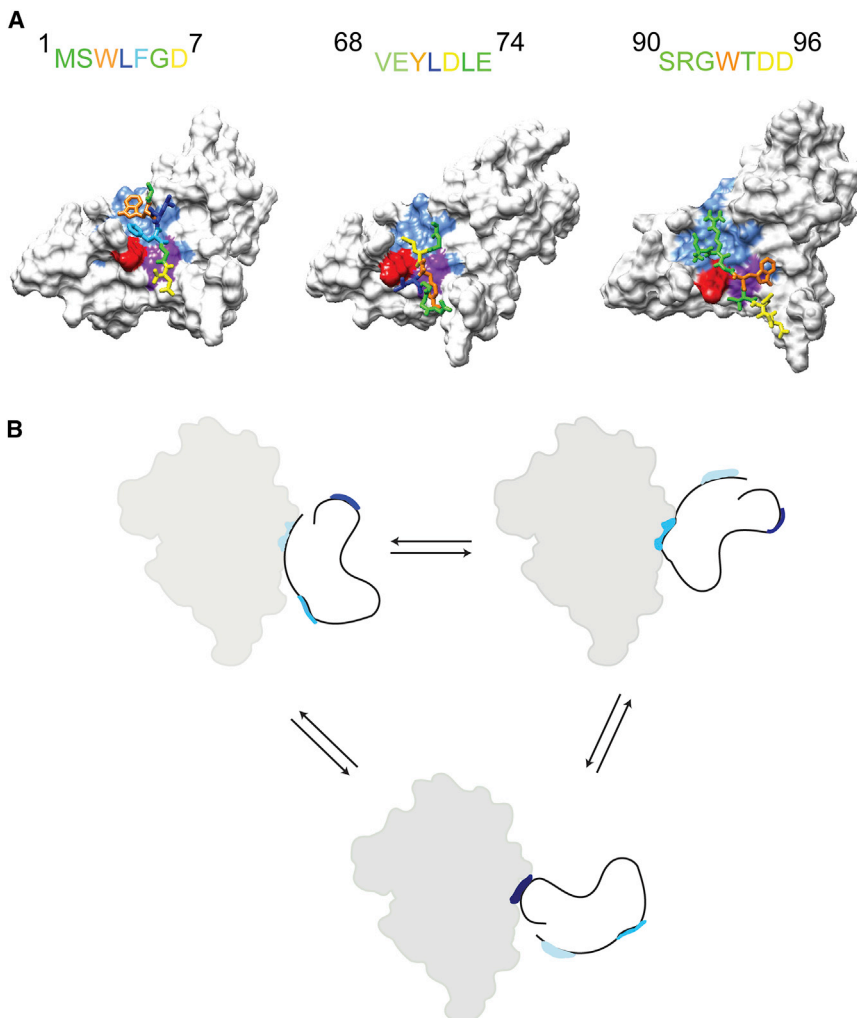


Figure 5. Dynamic Structure of the Tim21^{IMS}-Tim23^{IMS} Complex

(A) Structures of the interaction motifs of Tim23^{IMS} (represented as sticks) in complex with Tim21^{IMS} obtained by NMR-driven flexible peptide docking. On top, the primary sequence of the interaction motifs of Tim23^{IMS} is shown (color coding as in complex structure). K139 (red) and Y141 (purple) of Tim21 act as the main hydrophobic anchor.

(B) Schematic representation of the complex nature of the Tim23^{IMS}-Tim21^{IMS} interaction. Three interaction motifs of Tim23^{IMS} (colored blue, red, and purple) bind to a single binding pocket in Tim21^{IMS} (filled gray surface). Three representations are shown, highlighting that three interaction motifs of Tim23^{IMS} rapidly exchange with the Tim21^{IMS} binding pocket. By connection of three interaction motifs in one chain, the overall affinity toward Tim21 is increased. At the same time, the presence of multiple interaction motifs enables simultaneous binding to multiple partners and therefore dynamic regulation of complex formation.

the I-TASSER server (Zhang, 2008). The mutants Tim23^{IMS}(T11C), Tim23^{IMS}(G67C), and Tim21^{IMS}(S114C, C128A) were generated using the Quick Change Mutagenesis kit from Stratagene and were verified by DNA sequencing. All protein samples were dialyzed against NMR buffer (20 mM HEPES, 50 mM NaCl, pH = 7.2) prior to NMR studies.

Tom40(361–387), Tim23(1–13), and Tim23(61–96) were prepared by solid-phase synthesis. Tom40(361–387) as well as Tim23(61–96) were prepared as acetylated peptides at the N terminus, to avoid an additional charge at the N terminus (for example when compared to the corresponding motif in Tim23[1–96]). All three peptides were purified with reverse-phase HPLC.

For paramagnetic relaxation enhancement studies, a 5-fold molar excess of MTSL—(S-(2, 2, 5, 5-tetramethyl-2, 5-dihydro-1H-pyrrol-3-yl) methyl methanesulfonothioate—; purchased from Toronto Research Chemicals—was added to the protein and allowed to react for 2 hr at 4°C. Excess MTSL was removed using a PD-10 desalting column (GE Healthcare). After loading with MTSL, protein samples were dialyzed against NMR buffer (20 mM HEPES, 50 mM NaCl, pH = 7.2). The covalent attachment of MTSL to the protein of interest was confirmed with electrospray mass spectrometry.

NMR Spectroscopy

NMR spectra were recorded on 600 and 700 MHz Bruker spectrometers equipped with cryogenic probes (Bruker Biospin). NMR spectra of Tim23^{IMS} and Tim21^{IMS} were measured at 288 K and 298 K, respectively. NMR data were processed using NMR Pipe (Delaglio et al., 1995) and analyzed using SPARKY (T.D. Goddard and D.G. Kneller, University of California, San Francisco).

Sequence-specific resonance assignment of Tim21^{IMS} was accomplished using conventional 3D NMR experiments (HNCA, HNCACB, CBCACONH, HNCO, HCCH-TOCSY, ¹³C-edited NOESY-heteronuclear single-quantum correlation [HSQC], ¹⁵N edited-NOESY-HSQC; Sattler et al., 1999). The structure of Tim21^{IMS} was calculated using the distance restraints derived from ¹³C-edited NOESY-HSQC (aliphatic and aromatic) and ¹⁵N edited-NOESY-HSQC spectra. The 20 lowest-energy structures were further refined in explicit solvent using X-PLOR NIH (Schwieters et al., 2003).

¹⁵N-¹H HSQC spectra were recorded in the presence and absence of the ligand at different molar ratios using identical NMR acquisition parameters.

space domain of Tim23 in the formation and dynamic regulation of the presequence translocase.

EXPERIMENTAL PROCEDURES

Protein Preparation

Constructs corresponding to the IMS domains of Tim23(1–96), Tim50(164–361), Tim50(164–476), Tim21(103–225), and Tom22(120–153) were amplified from c-DNA templates obtained from the Harvard Plasmid Repository and were confirmed by DNA sequencing. Tim23(1–96) was expressed and purified as described earlier (de la Cruz et al., 2010), whereas all other constructs were fused with an N-terminal Z₂ domain using a modified pET28a vector (Bogomolovas et al., 2009). The growth medium was selected based on the type of sample needed, such as M9 medium supplemented by 4 g ¹³C glucose, 1 g ¹⁵N NH₄Cl for ¹³C ¹⁵N samples, and 1 g ¹⁵N NH₄Cl for ¹⁵N-labeled samples. For all constructs, protein expression in *Escherichia coli* BL21 (DE3) cells was induced with 1 mM isopropyl β-D-1-thiogalactopyranoside at an optical density 600 of 0.6. Tom22^{IMS} was expressed at 37°C for 5 hr, Tim21^{IMS} at 25°C for 10 hr, and Tim50^{IMS} at 16°C for 16 hr. The fusion proteins were purified using IMAC (Ni-NTA) followed by TEV cleavage at room temperature. The cleaved proteins were reloaded onto Ni-NTA beads to remove the Z₂ domain and TEV. Gel filtration on a Superdex 75 HiLoad column (GE Healthcare) was used to further purify Tim21^{IMS} and Tim50^{IMS}. Tom22^{IMS} was purified by reverse-phase high-performance liquid chromatography (HPLC). The N-terminal residues 361–387 of Tom40 were predicted to be disordered using

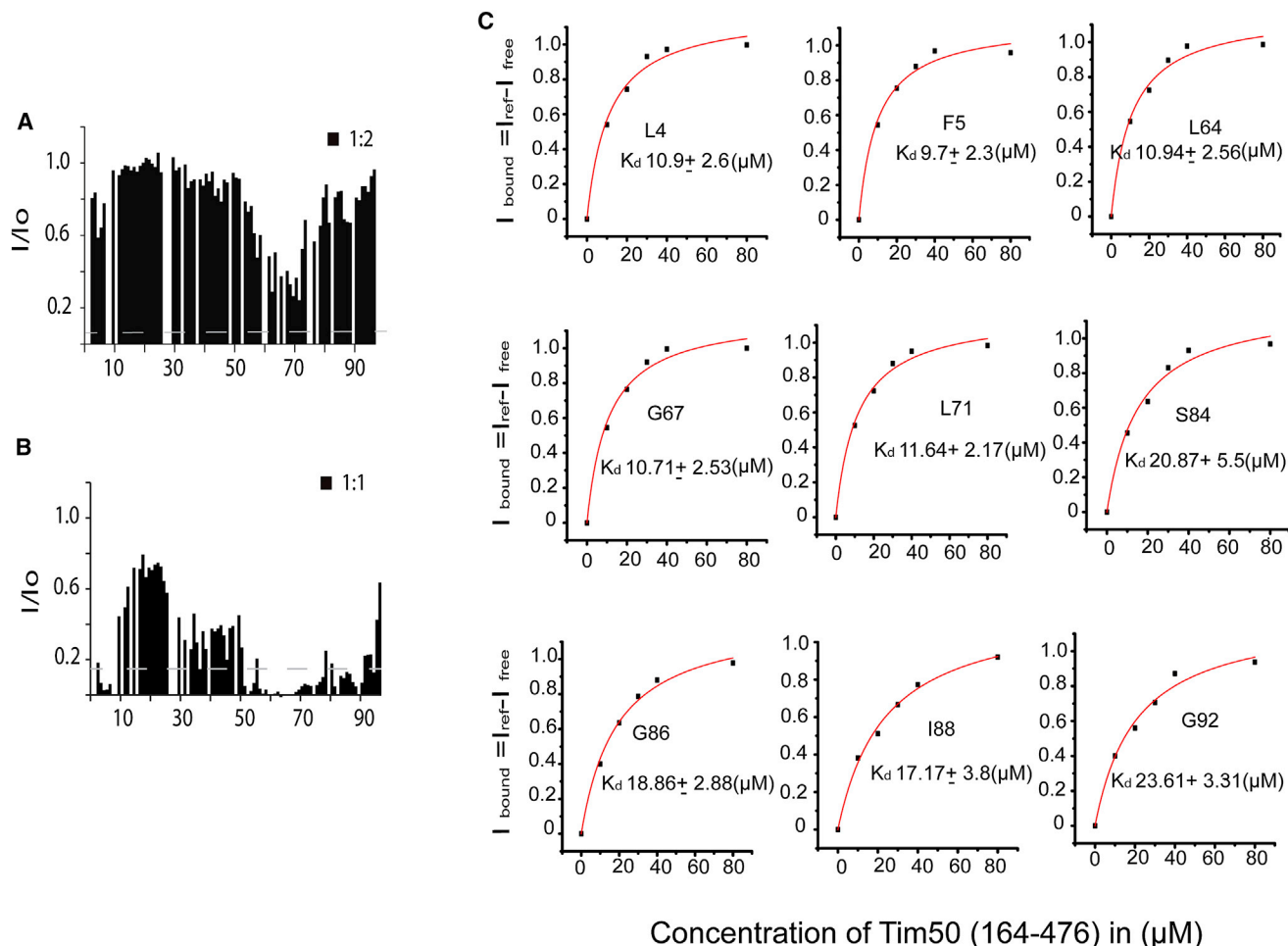


Figure 6. Recognition of Tim50 by Tim23

(A and B) Normalized NMR signal intensity changes (I/I_0) as a function of the primary sequence of Tim23^{IMS} at a 2-fold excess of Tim50(164–361) (A) and at an equimolar concentration of Tim50(164–476) (B). (C) Residue-specific binding curves for Tim23^{IMS} upon binding to Tim50(164–476). I_{bound} is the fraction of Tim23^{IMS} bound to Tim50(164–476) as obtained from NMR signal intensity changes in 2D ^1H - ^{15}N HSQC spectra of Tim23^{IMS} (I_{free}) upon addition of Tim50(164–476) (I_{ref}). The solid curve shows the fit to a single site binding model.

The normalized average chemical shift perturbation (CSP), Δ_{HN} , was calculated as $\Delta_{\text{HN}} = \{[(\delta_{\text{N}}/5)^2 + (\delta_{\text{H}})^2]^{1/2}\}$.

To determine the binding affinity, K_d , changes in CSP as a function of concentration of the ligand were fitted to a single-site binding model according to

$$\Delta_{\text{HN}} = \Delta\delta_{\text{max}} \left([L]_{\text{T}} + [P]_{\text{T}} + K_d - \left\{ ([L]_{\text{T}} + [P]_{\text{T}} + K_d)^2 - 4[L]_{\text{T}} * [P]_{\text{T}} \right\}^{1/2} \right) / (2[P]_{\text{T}}),$$

where $\Delta\delta_{\text{max}}$ is the maximal chemical shift perturbation value at saturation, and $[P]_{\text{T}}$ and $[L]_{\text{T}}$ are the total concentration of protein and ligand.

Intermolecular paramagnetic relaxation enhancement was determined based on ^1H - ^{15}N -HSQC spectra using samples that contained a 1:1 ratio of labeled protein and unlabeled binding partner. The diamagnetic state was measured with identical acquisition parameters after addition of ascorbic acid (10 molar equivalents to protein) to the same sample. The intensity error in each spectrum was obtained from the signal-to-noise ratio.

NMR-Based Docking of the Tim23^{IMS}-Tim21^{IMS} Complex

Peptides corresponding to the Tim21-interaction motifs of Tim23 ($^1\text{MSWLFGD}^7$, $^{68}\text{VEYLDLE}^{74}$, and $^{90}\text{SRGWTD}^{96}$) were manually placed 10–12 Å away from the binding site in Tim21^{IMS} (lowest energy conformer of the

NMR structure) according to the experimentally observed chemical shift perturbation and intermolecular paramagnetic relaxation enhancement data. Subsequently, the protein-peptide complex models were docked and refined using the FlexPepDock refinement protocol in Rosetta3.2 (Raveh et al., 2010, 2011). For each of the three interaction motifs, 25,000 decoys were created and ranked according to the reweighted Rosetta energy score. The top 500 models were then clustered using a backbone root-mean-square deviation (rmsd) of 2 Å. The top scoring five clusters were in agreement with PREs and CSP and were analyzed manually.

ACCESSION NUMBERS

The Protein Data Bank accession number for the structure coordinates of Tim21^{IMS} is 2MF7, and the BioMagRes Bank accession number for its chemical shifts is 19538.

SUPPLEMENTAL INFORMATION

Supplemental Information includes three figures and can be found with this article online at <http://dx.doi.org/10.1016/j.str.2014.07.015>.

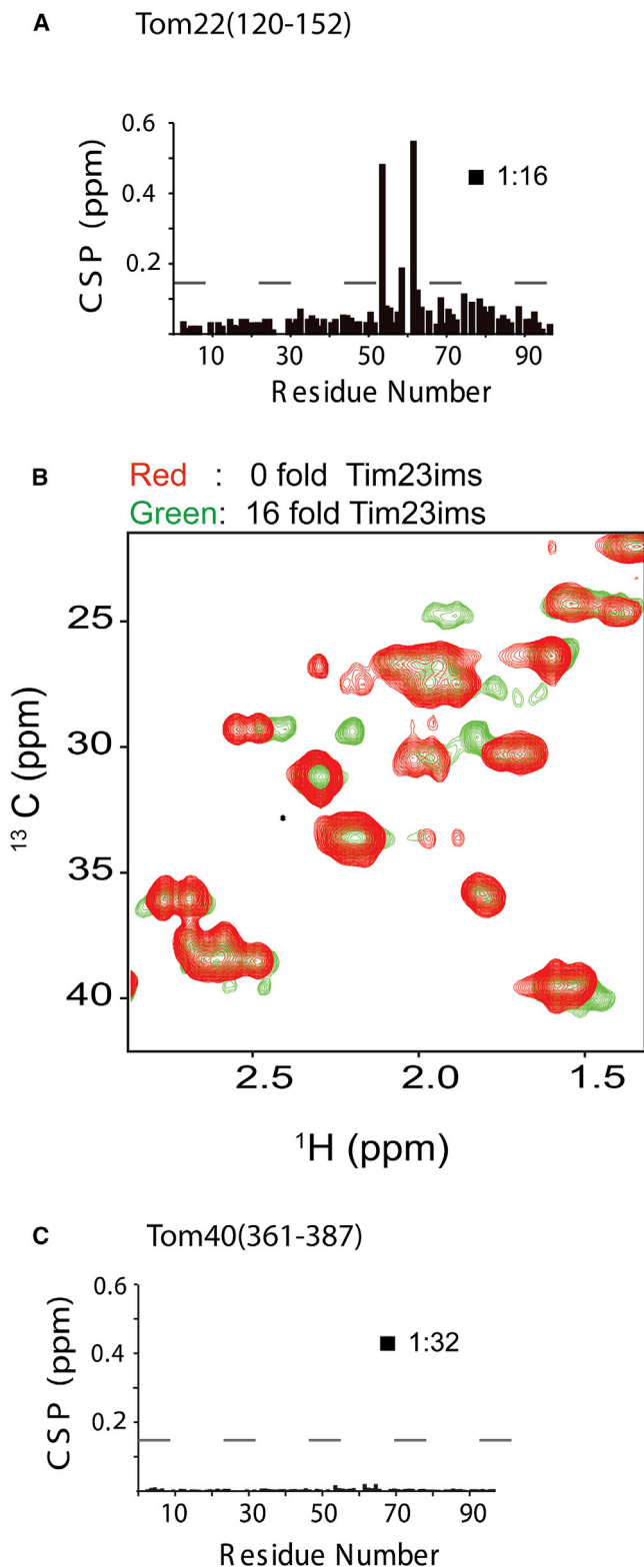


Figure 7. The Tim23-Tom22 Translocation Contact

(A) Tom22^{IMS} binds to a distinct site in the central region of Tim23^{IMS} as evidenced by ¹H-¹⁵N NMR chemical shift perturbation of Tim23^{IMS} in the presence of a 16-fold excess of Tom22^{IMS}. The gray dashed line indicates the estimated error in the chemical shift perturbation analysis.

AUTHOR CONTRIBUTIONS

R.B. prepared proteins and performed NMR experiments and analyzed data; Ł.J. and M.J. determined the Tim21^{IMS} structure; S.B. supervised the protein preparation; R.B. and M.Z. wrote the manuscript; and S.B. and M.Z. supervised the project.

ACKNOWLEDGMENTS

We thank Kerstin Overkamp for peptide synthesis and Peter Rehling for help in the initial phase of the project. This work was supported by the Foundation for Polish Science (Fundacja na rzecz Nauki Polskiej, FNP) START, the Ventures Programme (to M.J. and Ł.J.), and cofinanced by the EU European Regional Development Fund and the DFG Collaborative Research Center 860, project B2 (to M.Z.).

Received: November 21, 2013

Revised: July 4, 2014

Accepted: July 19, 2014

Published: September 25, 2014

REFERENCES

- Abe, Y., Shodai, T., Muto, T., Mihara, K., Torii, H., Nishikawa, S., Endo, T., and Kohda, D. (2000). Structural basis of presequence recognition by the mitochondrial protein import receptor Tom20. *Cell* *100*, 551–560.
- Albrecht, R., Rehling, P., Chacinska, A., Brix, J., Cadamuro, S.A., Volkmer, R., Guiard, B., Pfanner, N., and Zeth, K. (2006). The Tim21 binding domain connects the preprotein translocases of both mitochondrial membranes. *EMBO Rep.* *7*, 1233–1238.
- Bauer, M.F., Sirrenberg, C., Neupert, W., and Brunner, M. (1996). Role of Tim23 as voltage sensor and presequence receptor in protein import into mitochondria. *Cell* *87*, 33–41.
- Bauer, M.F., Hofmann, S., Neupert, W., and Brunner, M. (2000). Protein translocation into mitochondria: the role of TIM complexes. *Trends Cell Biol.* *10*, 25–31.
- Bogomolovas, J., Simon, B., Sattler, M., and Stier, G. (2009). Screening of fusion partners for high yield expression and purification of bioactive viscotoxins. *Protein Expr. Purif.* *64*, 16–23.
- Chacinska, A., Rehling, P., Guiard, B., Frazier, A.E., Schulze-Specking, A., Pfanner, N., Voos, W., and Meisinger, C. (2003). Mitochondrial translocation contact sites: separation of dynamic and stabilizing elements in formation of a TOM-TIM-preprotein supercomplex. *EMBO J.* *22*, 5370–5381.
- Chacinska, A., Lind, M., Frazier, A.E., Dudek, J., Meisinger, C., Geissler, A., Sickmann, A., Meyer, H.E., Truscott, K.N., Guiard, B., et al. (2005). Mitochondrial presequence translocase: switching between TOM tethering and motor recruitment involves Tim21 and Tim17. *Cell* *120*, 817–829.
- Chacinska, A., Koehler, C.M., Milenkovic, D., Lithgow, T., and Pfanner, N. (2009). Importing mitochondrial proteins: machineries and mechanisms. *Cell* *138*, 628–644.
- Clamp, M., Cuff, J., Searle, S.M., and Barton, G.J. (2004). The Jalview Java alignment editor. *Bioinformatics* *20*, 426–427.
- Davis, A.J., Sepuri, N.B., Holder, J., Johnson, A.E., and Jensen, R.E. (2000). Two intermembrane space TIM complexes interact with different domains of Tim23p during its import into mitochondria. *J. Cell Biol.* *150*, 1271–1282.
- de la Cruz, L., Bajaj, R., Becker, S., and Zweckstetter, M. (2010). The intermembrane space domain of Tim23 is intrinsically disordered with a distinct binding region for presequences. *Protein Sci.* *19*, 2045–2054.

(B) Superposition of selected regions from 2D ¹³C-¹H HSQC spectra of Tom22^{IMS} in the presence (green) and absence (red) of Tim23^{IMS}.

(C) Influence of addition of Tom40(361-387) on ¹H-¹⁵N HSQC spectra of Tim23^{IMS}. Chemical shifts remained below the estimated uncertainty (gray dashed line) indicating that Tom40(361-387) does not bind to Tim23^{IMS} in vitro.

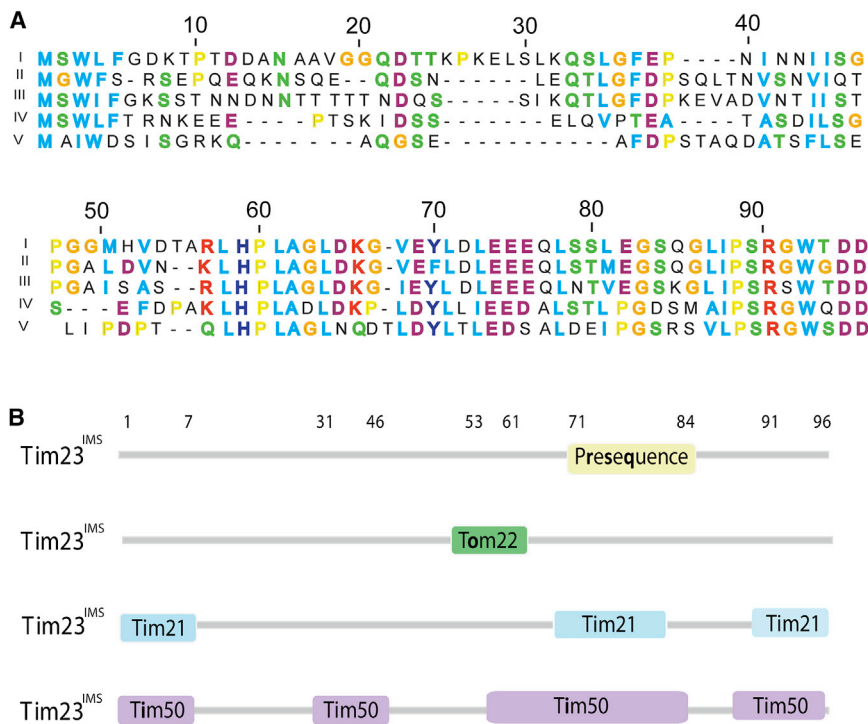


Figure 8. Protein Interaction Network of Tim23^{IMS}

(A) Sequence alignment for Tim23^{IMS} highlighting the conservation of residues among different Fungi kingdoms with 1-5 as *S. cerevisiae*, *ZygoSaccharomyces rouxii*, *Candida albicans*, *Schizosaccharomyces pombe*, and *Aspergillus fumigatus*, respectively. Hydrophobic and aromatic residues are highlighted in blue; positive and negative charged residues are shown in red and magenta, respectively; neutral residues in green; and glycine and proline in orange and yellow, respectively.

(B) Summary of interaction motifs in Tim23^{IMS} used for binding to Tim21^{IMS}, Tom22^{IMS}, presequence (de la Cruz et al., 2010), and Tim50^{IMS}. Each interaction motif is used for binding to multiple protein partners.

Delaglio, F., Grzesiek, S., Vuister, G.W., Zhu, G., Pfeifer, J., and Bax, A. (1995). NMRPipe: a multidimensional spectral processing system based on UNIX pipes. *J. Biomol. NMR* 6, 277–293.

Donzeau, M., Káldi, K., Adam, A., Paschen, S., Wanner, G., Guiard, B., Bauer, M.F., Neupert, W., and Brunner, M. (2000). Tim23 links the inner and outer mitochondrial membranes. *Cell* 101, 401–412.

Endo, T., Yamano, K., and Kawano, S. (2011). Structural insight into the mitochondrial protein import system. *Biochim. Biophys. Acta* 1808, 955–970.

Gebert, M., Schrempf, S.G., Mehnert, C.S., Heißwolf, A.K., Oeljeklaus, S., Ieva, R., Bohnert, M., von der Malsburg, K., Wiese, S., Kleinschroth, T., et al. (2012). Mgr2 promotes coupling of the mitochondrial presequence translocase to partner complexes. *J. Cell Biol.* 197, 595–604.

Geissler, A., Chacinska, A., Truscott, K.N., Wiedemann, N., Brandner, K., Sickmann, A., Meyer, H.E., Meisinger, C., Pfanner, N., and Rehling, P. (2002). The mitochondrial presequence translocase: an essential role of Tim50 in directing preproteins to the import channel. *Cell* 111, 507–518.

Gevorkyan-Airapetov, L., Zohary, K., Popov-Celeketi, D., Mapa, K., Hell, K., Neupert, W., Azem, A., and Mokranjac, D. (2009). Interaction of Tim23 with Tim50 Is essential for protein translocation by the mitochondrial TIM23 complex. *J. Biol. Chem.* 284, 4865–4872.

Glick, B.S., Brandt, A., Cunningham, K., Müller, S., Hallberg, R.L., and Schatz, G. (1992). Cytochromes c1 and b2 are sorted to the intermembrane space of yeast mitochondria by a stop-transfer mechanism. *Cell* 69, 809–822.

Hutu, D.P., Guiard, B., Chacinska, A., Becker, D., Pfanner, N., Rehling, P., and van der Laan, M. (2008). Mitochondrial protein import motor: differential role of Tim44 in the recruitment of Pam17 and J-complex to the presequence translocase. *Mol. Biol. Cell* 19, 2642–2649.

Komuro, Y., Miyashita, N., Mori, T., Muneyuki, E., Saitoh, T., Kohda, D., and Sugita, Y. (2013). Energetics of the presequence-binding poses in mitochondrial protein import through Tom20. *J. Phys. Chem. B* 117, 2864–2871.

Koradi, R., Billeter, M., and Wüthrich, K. (1996). MOLMOL: a program for display and analysis of macromolecular structures. *J. Mol. Graph.* 14, 51–55, 29–32.

Kutik, S., Guiard, B., Meyer, H.E., Wiedemann, N., and Pfanner, N. (2007). Cooperation of translocase complexes in mitochondrial protein import. *J. Cell Biol.* 179, 585–591.

Larkin, M.A., Blackshields, G., Brown, N.P., Chenna, R., McGettigan, P.A., McWilliam, H., Valentin, F., Wallace, I.M., Wilm, A., Lopez, R., et al. (2007). Clustal W and Clustal X version 2.0. *Bioinformatics* 23, 2947–2948.

Laskowski, R.A., Rullmann, J.A., MacArthur, M.W., Kaptein, R., and Thornton, J.M. (1996). AQUA and PROCHECK-NMR: programs for checking the quality of protein structures solved by NMR. *J. Biomol. NMR* 8, 477–486.

Lytovchenko, O., Melin, J., Schulz, C., Kilisch, M., Hutu, D.P., and Rehling, P. (2013). Signal recognition initiates reorganization of the presequence translocase during protein import. *EMBO J.* 32, 886–898.

Marom, M., Dayan, D., Demishtein-Zohary, K., Mokranjac, D., Neupert, W., and Azem, A. (2011). Direct interaction of mitochondrial targeting presequences with purified components of the TIM23 protein complex. *J. Biol. Chem.* 286, 43809–43815.

Martinez-Caballero, S., Grigoriev, S.M., Herrmann, J.M., Campo, M.L., and Kinnally, K.W. (2007). Tim17p regulates the twin pore structure and voltage gating of the mitochondrial protein import complex TIM23. *J. Biol. Chem.* 282, 3584–3593.

Meinecke, M., Wagner, R., Kovermann, P., Guiard, B., Mick, D.U., Hutu, D.P., Voos, W., Truscott, K.N., Chacinska, A., Pfanner, N., and Rehling, P. (2006). Tim50 maintains the permeability barrier of the mitochondrial inner membrane. *Science* 312, 1523–1526.

Mittag, T., Orlicky, S., Choy, W.Y., Tang, X., Lin, H., Sicheri, F., Kay, L.E., Tyers, M., and Forman-Kay, J.D. (2008). Dynamic equilibrium engagement of a polyvalent ligand with a single-site receptor. *Proc. Natl. Acad. Sci. USA* 105, 17772–17777.

Moczko, M., Bömer, U., Kübrich, M., Zufall, N., Hönlinger, A., and Pfanner, N. (1997). The intermembrane space domain of mitochondrial Tom22 functions as a trans binding site for preproteins with N-terminal targeting sequences. *Mol. Cell. Biol.* 17, 6574–6584.

- Mokranjac, D., Paschen, S.A., Kozany, C., Prokisch, H., Hoppins, S.C., Nargang, F.E., Neupert, W., and Hell, K. (2003). Tim50, a novel component of the TIM23 preprotein translocase of mitochondria. *EMBO J.* **22**, 816–825.
- Mokranjac, D., Popov-Celeketić, D., Hell, K., and Neupert, W. (2005). Role of Tim21 in mitochondrial translocation contact sites. *J. Biol. Chem.* **280**, 23437–23440.
- Neupert, W., and Herrmann, J.M. (2007). Translocation of proteins into mitochondria. *Annu. Rev. Biochem.* **76**, 723–749.
- Pfanner, N. (1998). Mitochondrial import: crossing the aqueous intermembrane space. *Curr. Biol.* **8**, R262–R265.
- Pfanner, N., and Geissler, A. (2001). Versatility of the mitochondrial protein import machinery. *Nat. Rev. Mol. Cell Biol.* **2**, 339–349.
- Popov-Celeketić, D., Mapa, K., Neupert, W., and Mokranjac, D. (2008). Active remodelling of the TIM23 complex during translocation of preproteins into mitochondria. *EMBO J.* **27**, 1469–1480.
- Qian, X., Gebert, M., Höpker, J., Yan, M., Li, J., Wiedemann, N., van der Laan, M., Pfanner, N., and Sha, B. (2011). Structural basis for the function of Tim50 in the mitochondrial presequence translocase. *J. Mol. Biol.* **411**, 513–519.
- Raveh, B., London, N., and Schueler-Furman, O. (2010). Sub-angstrom modeling of complexes between flexible peptides and globular proteins. *Proteins* **78**, 2029–2040.
- Raveh, B., London, N., Zimmerman, L., and Schueler-Furman, O. (2011). Rosetta FlexPepDock ab-initio: simultaneous folding, docking and refinement of peptides onto their receptors. *PLoS ONE* **6**, e18934.
- Ryan, K.R., and Jensen, R.E. (1995). Protein translocation across mitochondrial membranes: what a long, strange trip it is. *Cell* **83**, 517–519.
- Saitoh, T., Igura, M., Miyazaki, Y., Ose, T., Maita, N., and Kohda, D. (2011). Crystallographic snapshots of Tom20-mitochondrial presequence interactions with disulfide-stabilized peptides. *Biochemistry* **50**, 5487–5496.
- Sattler, M., Schleucher, J., and Griesinger, C. (1999). Heteronuclear multidimensional NMR experiments for the structure determination of proteins in solution employing pulsed field gradients. *Prog. Nucl. Magn. Reson. Spectrosc.* **34**, 93–158.
- Schatz, G. (1996). The protein import system of mitochondria. *J. Biol. Chem.* **271**, 31763–31766.
- Schulz, C., Lytovchenko, O., Melin, J., Chacinska, A., Guiard, B., Neumann, P., Ficner, R., Jahn, O., Schmidt, B., and Rehling, P. (2011). Tim50's presequence receptor domain is essential for signal driven transport across the TIM23 complex. *J. Cell Biol.* **195**, 643–656.
- Schwieters, C.D., Kuszewski, J.J., Tjandra, N., and Clore, G.M. (2003). The Xplor-NIH NMR molecular structure determination package. *J. Magn. Reson.* **160**, 65–73.
- Shiota, T., Mabuchi, H., Tanaka-Yamano, S., Yamano, K., and Endo, T. (2011). In vivo protein-interaction mapping of a mitochondrial translocator protein Tom22 at work. *Proc. Natl. Acad. Sci. USA* **108**, 15179–15183.
- Tamura, Y., Harada, Y., Shiota, T., Yamano, K., Watanabe, K., Yokota, M., Yamamoto, H., Sesaki, H., and Endo, T. (2009). Tim23-Tim50 pair coordinates functions of translocators and motor proteins in mitochondrial protein import. *J. Cell Biol.* **184**, 129–141.
- Truscott, K.N., Kovermann, P., Geissler, A., Merlin, A., Meijer, M., Driessen, A.J., Rassow, J., Pfanner, N., and Wagner, R. (2001). A presequence- and voltage-sensitive channel of the mitochondrial preprotein translocase formed by Tim23. *Nat. Struct. Biol.* **8**, 1074–1082.
- van der Laan, M., Meinecke, M., Dudek, J., Hutu, D.P., Lind, M., Perschil, I., Guiard, B., Wagner, R., Pfanner, N., and Rehling, P. (2007). Motor-free mitochondrial presequence translocase drives membrane integration of preproteins. *Nat. Cell Biol.* **9**, 1152–1159.
- van der Laan, M., Hutu, D.P., and Rehling, P. (2010). On the mechanism of preprotein import by the mitochondrial presequence translocase. *Biochimica et Biophysica Acta (BBA) - Mol. Cell Res.* **1803**, 732–739.
- Wiedemann, N., Frazier, A.E., and Pfanner, N. (2004). The protein import machinery of mitochondria. *J. Biol. Chem.* **279**, 14473–14476.
- Yamamoto, H., Esaki, M., Kanamori, T., Tamura, Y., Nishikawa, S., and Endo, T. (2002). Tim50 is a subunit of the TIM23 complex that links protein translocation across the outer and inner mitochondrial membranes. *Cell* **111**, 519–528.
- Zhang, Y. (2008). I-TASSER server for protein 3D structure prediction. *BMC Bioinformatics* **9**, 40.